AIAA 80-0383aR

Improved Calculation of High Speed Inlet Flows: Part I. Numerical Algorithm

Doyle D. Knight*
Rutgers University, New Brunswick, N.J.

An improved numerical algorithm has been developed for the calculation of flowfields in two-dimensional high speed inlets. The full mean compressible Navier-Stokes equations are employed, with turbulence represented by an algebraic turbulent eddy viscosity. A body-oriented coordinate transformation is used to facilitate treatment of arbitrary inlet contours. The explicit finite-difference algorithm of MacCormack is utilized. Several well-known techniques for improving computational efficiency are incorporated, including time-splitting of the finite-difference operators and splitting of the mesh into several regions in the cross-stream direction. A number of new computational techniques are introduced; namely, a procedure for automatic determination of the optimal mesh splitting, and a separate treatment of the viscous sublayer and transition wall region of the turbulent boundary layers. The accuracy and efficiency of the approach is demonstrated for the specific examples of the development of a turbulent boundary layer on a flat plate, and the interaction of a shock wave with a flat plate turbulent boundary layer. In all cases, the results compare very favorably with previous numerical calculations and experimental results.

Nomenclature

c_f	= skin friction coefficient
D	= Van Driest damping factor
e	= total energy per unit mass
$\mathcal{F},\mathcal{G}$	= flux vectors in ζ and η directions, respectively
$\dot{m}$	= bleed mass flux
N	= modification to D due to mass bleed
p	= static pressure
Q_x, Q_y	= Cartesian components of heat transfer vector
$Q_{x'}, Q_{y'}$	= components of heat transfer vector in x', y' system
t	= time
$\mathcal{U}$	= vector of dependent variables
u_*	= friction velocity, $u_* = \sqrt{\tau_w/\rho_w}$
u,v	= Cartesian components of velocity
u',v'	= components of velocity in x',y' system
x,y	= Cartesian coordinates
x',y'	= locally orthogonal coordinates at boundary
y'_m	= height of computational sublayer
$\Delta\zeta,\Delta\eta$	= mesh spacing in ζ and η directions
α	= pressure damping coefficient
δ	= boundary-layer thickness
ϵ	= turbulent eddy viscosity
ζ,η	= transformed coordinates
ν	= kinematic viscosity, $\nu = \mu/\rho$
ρ	= density
$\tau_{xx}, \tau_{xy}, \tau_{yy}$	= components of Cartesian stress tensor in x,y system
$\tau_{x'x'}, \tau_{x'y'}, \tau_{y'y'}$	= components of Cartesian stress tensor in x',y' system

Subscripts

w	= evaluated at wall
∞	= evaluated upstream of body

Received Nov. 15, 1979; presented as part of Paper 80-0383 at the AIAA 18th Aerospace Sciences Meeting, Pasadena, Calif., Jan. 14-16, 1980; revision received June 20, 1980.

*Assistant Professor, Department of Mechanical, Industrial and Aerospace Engineering. Member AIAA.

Introduction

THE accurate prediction of the performance of high-speed inlets is an important and challenging aspect of modern high-speed aircraft design. The function of a jet engine inlet is to provide a nearly uniform subsonic flow with high total pressure recovery at the compressor face at minimal drag penalty.[1] A supersonic inlet flowfield is characterized by a pattern of oblique shock waves, formed by the general curvilinear shape of the ramp and cowl surfaces, that interact with the turbulent boundary layers on the walls. The shock wave train is usually terminated by an approximately normal shock (the "terminal shock") positioned at or near the inlet throat. Boundary-layer bleed is generally provided on the ramp, cowl, and sidewalls to prevent flow separation in the vicinity of the intersection of the shock waves and walls.

Traditionally, theoretical inlet design and analysis has been based on the separate, and sometimes coupled, treatment of the inviscid and viscous portions of the inlet flow. The calculation of the inviscid flow is accomplished either by the conventional method of characteristics[2,3] or inviscid finite-difference shock-capturing techniques.[4] The effect of the boundary-layer displacement thickness is either ignored[3-5] or incorporated as a correction.[6] The calculation of the wall boundary layers typically involves a finite-difference solution of the boundary-layer equations with a semiempirical model of shock/boundary-layer interaction.[6,7] The determination of bounary-layer bleed necessary to prevent flow separation typically is achieved by means of empirical criteria based on the velocity profile.[7,8]

The traditional approach, however, suffers from three major disadvantages. First of all, the use of semiempirical models of shock/boundary-layer interaction oftentimes yields incorrect predictions of the reflected shock wave structure and consequently unreliable performance predictions.[6,9] Second, the conventional method of characteristics and inviscid finite-difference shock-capturing techniques are limited to regions of supersonic flow.[2-4,6] In practice, both methods perform a marching operation in the downstream direction beginning at the inlet entrance. The development of any region of subsonic flow terminates the computations, which in practice sometimes may occur upstream of the inlet throat.[4,6] Also, the interaction of the terminal shock with the boundary layers and the subsonic diffuser flowfield cannot be treated by these techniques. Third, these methods are incapable of handling flow separation due to their inadequate treatment of strong

viscous-inviscid interactions. The presence of large flow separation within inlets at high angle of attack is a major concern for aircraft designers.[10]

Some of the disadvantages of the traditional approach can be overcome by using the "parabolized" Navier-Stokes equations, which are obtained from the full Navier-Stokes equations by neglecting diffusion in the primary flow direction.[11] The technique is based on performing a single sweep marching operation in the primary flow direction, and consequently requires substantially less computer time and storage than the methods discussed later that employ the time-dependent Navier-Stokes equations. The primary application of the technique in high-speed flows has been to external flowfields,[11,12] although recently high-speed inlets have been treated.[13] Since the method is based on a single sweep marching operation in the streamwise direction, it is incapable of incorporating boundary conditions at the downstream end of the computational domain such as the specification of the downstream or "back" pressure. Consequently, the technique is evidently incapable of computing the terminal shock and subsequent subsonic diffuser flowfield, as well as high-speed inlet flows exhibiting inlet unstart (i.e., terminal shock moving upstream of the inlet entrance). Furthermore, the assumptions of the technique are invalid in the presence of streamwise flow separation, although separation in the cross-flow plane can be handled.[12,13]

All of the disadvantages of the traditional approach can be overcome by utilizing the time-dependent Navier-Stokes equations and simultaneously treating the entire inlet flowfield (or, in some cases, subregions of the inlet flowfield as discussed later). The steady inlet flowfield typically is obtained by integration in time from an assumed initial condition until the steady state is achieved. Unsteady inlet flows may also be treated. In recent years, accurate calculation of high-speed flows with shock/boundary-layer interaction and streamwise flow separation has been demonstrated using a variety of numerical algorithms for the time-dependent Navier-Stokes equations. A brief sampling includes MacCormack's explicit[14-17] and hybrid implicit-explicit[18] methods, the hybrid implicit-explicit method of Shang,[19] and the implicit method of Beam and Warming.[20-22] Both the hybrid and fully implicit methods have demonstrated substantial improvements in computational efficiency over the explicit approach. The capability for handling terminal shock structures and the subsequent downstream subsonic diffuser flow has been demonstrated.[23]

To the author's knowledge, the first calculation of a realistic high-speed inlet using the Navier-Stokes equations is that of the author[24] using the explicit method of MacCormack.[14] The computed results compared very favorably with the experimental data for ramp and cowl static pressures and boundary-layer pitot profiles. The computer time requirements, however, were substantial, and the need for improved computational efficiency was the primary motivation for the present work. Quite recently, a modified form of the implicit method of Beam and Warming has been applied to the calculation of a low Reynolds number laminar supersonic inlet flow.[25] Although there was no comparison made with experimental data, the results are quite promising.

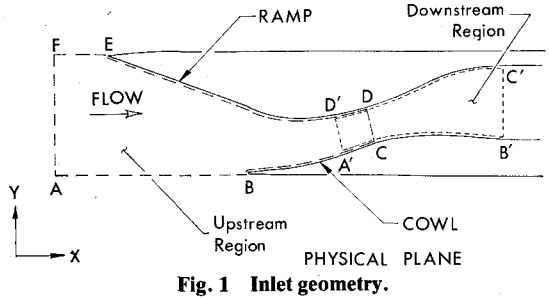

Fig. 1 Inlet geometry.

The focus of the present work is the development of a more efficient numerical algorithm for the prediction of two-dimensional high-speed inlets using the Navier-Stokes equations. A substantial improvement in computational efficiency has been achieved by incorporating a separate algorithm for the treatment of the viscous sublayer and transition wall region of the turbulent boundary layers. In this paper, the details of the numerical algorithm are provided, and several test cases are discussed. In the subsequent paper,[26] calculations are presented for a simulated two-dimensional mixed compression high-speed inlet.

Method of Solution

Coordinate Transformation

In order to facilitate treatment of a general curvilinear inlet geometry, a numerical coordinate transformation is employed whose purpose is to provide a set of curvilinear coordinates $\zeta(x,y)$ and $\eta(x,y)$ that are contoured to the inlet shape. The technique is illustrated in Fig. 1, where two overlapping computational regions ABCDEF (the upstream region) and A'B'C'D' (the downstream region) are indicated (the purpose of the overlapping regions is discussed later). In the upstream region, for example, the cowl and ramp surfaces are taken to be coincident with portions of the contours $\eta=0$ and $\eta=1$, respectively (Figs. 1 and 2). The upstream and downstream boundaries (curves AF and CD, respectively) are taken to be coincident with the contours $\zeta=0$ and $\zeta=1$, respectively. The η coordinate increases in a general cross-stream direction, while the ζ coordinate increases in the general streamwise direction. The coordinates are obtained from the following equations[27]:

$$\nabla^2\zeta=0, \qquad \nabla^2\eta=Q(\zeta,\eta) \tag{1}$$

where ∇^2 is the Laplacian operator $\partial^2/\partial x^2+\partial^2/\partial y^2$. The function Q is chosen to provide an approximately exponentially stretched mesh within the boundary layers on the ramp and cowl. Details are provided in Refs. 24 and 28. The coordinates ζ and η are subject to Dirichlet boundary conditions, implying that the coordinate transformation is not necessarily orthogonal. Accurate flowfield solutions can be obtained using coordinates exhibiting a modest degree of nonorthogonality.[24] For the calculations presented herein, an orthogonal coordinate system was used. In the inlet cases discussed in the subsequent paper,[26] the maximum derivation from orthogonality at any point is 10 deg. In practice, Eqs. (1) are inverted to solve for $x(\zeta,\eta)$ and $y(\zeta,\eta)$ and solved in the transformed plane.[27]

The result of the coordinate transformation is a uniform rectilinear grid of points in the transformed plane with constant mesh spacing $\Delta\zeta$ and $\Delta\eta$, whose image in the physical plane is a highly nonuniform grid capable of resolving the significant features of the flowfield. The Navier-Stokes equations are solved in the transformed plane, and the inlet flowfield in the physical plane is obtained through knowledge of the inverse transformation $x(\zeta,\eta)$ and $y(\zeta,\eta)$.

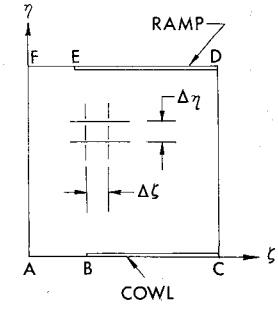

Fig. 2 Transformed plane (upstream region shown).

Governing Equations and Boundary Conditions

The governing equations are the full mean compressible Navier-Stokes equations using mass-averaged variables[29] for two-dimensional turbulent flow. Written in strong conservation form using the transformed coordinates $\xi(x,y)$ and $\eta(x,y)$, the equations are[21]

$$\frac{\partial \mathfrak{U}}{\partial t}+\frac{\partial \mathfrak{F}}{\partial \xi}+\frac{\partial \mathfrak{G}}{\partial \eta}=0 \tag{2}$$

where

$$\mathfrak{U}=\frac{1}{J}\begin{Bmatrix}\rho\\ \rho u\\ \rho v\\ \rho e\end{Bmatrix}$$

$$\mathfrak{F}=\frac{1}{J}\begin{Bmatrix}\rho U\\ \rho uU+\xi_x(p-\tau_{xx})-\xi_y\tau_{xy}\\ \rho vU+\xi_y(p-\tau_{yy})-\xi_x\tau_{xy}\\ (\rho e+p)U+\xi_x\beta_x+\xi_y\beta_y\end{Bmatrix}$$

$$\mathfrak{G}=\frac{1}{J}\begin{Bmatrix}\rho V\\ \rho uV+\eta_x(p-\tau_{xx})-\eta_y\tau_{xy}\\ \rho vV+\eta_y(p-\tau_{yy})-\eta_x\tau_{xy}\\ (\rho e+p)V+\eta_x\beta_x+\eta_y\beta_y\end{Bmatrix}$$

where ξ_x denotes $\partial\xi/\partial x$, etc. The quantities u and v denote the Cartesian x and y velocity components, respectively. The density ρ, pressure p, and temperature T are related through the equation of state $p=\rho RT$ where R is the gas constant. The total energy per unit mass e is given by $e=e_i+\frac{1}{2}(u^2+v^2)$ where the internal energy e_i is equal to c_vT. The contravariant velocity components U and V, the Jacobian J, and components of the total (laminar plus turbulent) Cartesian stress tensor (i.e., $\tau_{xx},\tau_{xy},\tau_{yy}$) are given in Ref. 28.

The quantities β_x and β_y are

$$\beta_x=Q_x-u\tau_{xx}-v\tau_{xy},\quad \beta_y=Q_y-u\tau_{xy}-v\tau_{yy} \tag{3}$$

where Q_x and Q_y are components of the total (laminar plus turbulent) heat flux vector.[28] The molecular dynamic viscosity is given by Sutherland's relation. The molecular Prandtl number Pr is 0.72 (air) and the turbulent Prandtl number Pr_t is 0.9.

The turbulent eddy viscosity ϵ is given by the two-layer equilibrium eddy viscosity of Cebeci and Smith[30] with the transition model of Dhawan and Narasimha.[28] For the high-speed inlet calculations, the location and extent of the region of transition from laminar to turbulent flow were estimated using the method of Deem and Murphy and the generally accepted criterion that the Reynolds number based on distance from the leading edge approximately doubles across the transition region.[28] The turbulent eddy viscosity relaxation model of Shang and Hankey[16] is incorporated for use in the vicinity of strong shock wave-turbulent boundary-layer interaction. The relaxation model was not employed, however, for shock/boundary-layer interactions in the presence of boundary-layer bleed, due to the lack of previous experience for such a configuration. The Van Driest damping factor D used in the inner equilibrium eddy viscosity is given by

$$D=1-\exp\left[-\frac{n\sqrt{|\tau_w|\rho_w}}{26\mu_w}N\right] \tag{4}$$

where n is the normal distance from the wall and N is a modification due to mass bleed

$$N=\exp\left[5.9\frac{\mu_w\dot{m}}{\mu\sqrt{|\tau_w|\rho_w}}\right] \tag{5}$$

where $\dot{m}$ is the normal mass flux at the wall. The pressure gradient term in N is omitted in agreement with several previous investigations.[16,17,28]

For the purposes of computational economy, the inlet flowfield is subdivided into two or more overlapping regions (see Fig. 1). Beginning with the upstream region, the flow in each region is converged to a steady state. The values of the flowfield variables at the restart station A′D′ are then used as the upstream profile for the next region. The application of this technique requires that within the overlapping region A′CDD′ the flowfield outside the boundary layers must be supersonic, and that the boundary layers are developing smoothly. The first requirement implies that the region extending from the inlet throat to the compressor face containing the terminal shock and subsonic diffuser must be handled by a single computational region. The second requirement indicates that the restart station cannot coincide with any strong viscous-inviscid interaction on the cowl or ramp. The technique of overlapping mesh regions has been widely used in high-speed flow calculations.[14-17,23,24]

The boundary conditions for Eq. (2) can be grouped into four categories. First, on the upstream boundary AF or restart station A′D′ in Fig. 1 the flow variables are held fixed at the appropriate freestream or converged upstream overlapping calculated values, respectively. Second, on the downstream boundaries CD and B′C′ the conventional zero-gradient boundary condition $\partial\mathfrak{U}/\partial\xi=0$ is applied. Third, on the cowl and ramp surfaces the boundary conditions are

$$\begin{aligned}
&v\cdot s=0 && \text{(no slip condition)}\\
&v\cdot n=v_w && \text{(boundary-layer bleed)}\\
&\frac{\partial T}{\partial n}=0 && \text{(adiabatic wall)}\\
&\frac{\partial p}{\partial n}=0 && \text{(approximate derived boundary condition for } p\text{)}
\end{aligned} \tag{6}$$

where s and n are tangential and normal unit vectors, respectively, at the wall v_w is the normal velocity at the wall. Fourth, for all calculations performed the flow in the vicinity of contours AB and EF is supersonic, and the following no reflection boundary conditions are employed

$$\frac{\partial u}{\partial \xi}=\frac{\partial v}{\partial \xi}=\frac{\partial T}{\partial \xi}=\frac{\partial p}{\partial \xi}=0 \tag{7}$$

where the derivative $\partial/\partial\xi$ is taken along the outward running characteristic at the boundary that is oriented at the local Mach angle with respect to the local velocity vector.

Numerical Algorithm

The explicit finite-difference algorithm of MacCormack[14,15] is employed to integrate Eq. (2) in time from an assumed initial condition until a steady-state flowfield is obtained. The algorithm is an alternating-direction technique of second-order accuracy, and has been employed in a wide variety of problems in high-speed flows involving strong viscous-inviscid interaction.[14-17,23,24] The procedure consists of repetitive application of an explicit finite-difference operator $\mathfrak{L}(\Delta t)$ to the vector of dependent variables $\mathfrak{U}$. The operator $\mathfrak{L}(\Delta t)$ is a symmetric sequence of time-split one-dimensional finite-difference operators $\mathfrak{L}_\xi(\Delta t_\xi)$ and

$\mathcal{L}_\eta(\Delta t_\eta)$. Each application of the operator $\mathcal{L}(\Delta t)$ updates $\mathcal{U}$ in time by an amount Δt. Details are provided in Ref. 28. For purposes of computational efficiency, the computational region is divided in the η direction into five subregions as indicated in Fig. 3. For the results discussed in this paper, the code was modified to use only regions 1-3, while for the results discussed in the subsequent paper,[26] all five regions were used. Within these subregions, the operator $\mathcal{L}(\Delta t)$ is given by

Regions 1, 2, 4, 5,

$$\mathcal{L}(\Delta t) = [\mathcal{L}_\eta(\Delta t/2m_\ell)\mathcal{L}_\xi(\Delta t/m_\ell)\mathcal{L}_\eta(\Delta t/2m_\ell)]^{m_\ell}$$

$$\ell = 1,2,4,5 \tag{8}$$

Region 3

$$\mathcal{L}(\Delta t) = \mathcal{L}_\xi(\Delta t/2)\mathcal{L}_\eta(\Delta t)\mathcal{L}_\xi(\Delta t/2)$$

where $m_\ell, \ell = 1,\ldots,5$ are integers with $m_3 \equiv 1$) and the exponent m_ℓ implies that the operator sequence within the brackets is applied m_ℓ times. The integers m_ℓ and time step Δt are determined by the requirement of numerical stability of the operators $\mathcal{L}_\xi$ and $\mathcal{L}_\eta$ in each of the five subregions.[15] A further requirement is that the ratios m_1/m_2 and m_5/m_4 be integers, in order that adjacent regions may be updated in time in a near simultaneous fashion.

An automatic optimization algorithm is utilized to determine the most efficient splitting of the five subregions at each time based on maximizing the ratio

$$\Delta t \Big/ \sum_{\ell=1}^{5} P_\ell m_\ell \tag{9}$$

where P_ℓ is the number of rows (i.e., η = constant mesh lines) in region ℓ. This quantity is essentially proportional to the ratio of the time step Δt to the computer time required to update the flowfield by the amount Δt, and thus is a direct measure of the relative efficiency of a particular mesh splitting. During the course of a calculation, the boundaries of the five subregions are automatically adjusted according to Eq. (9). There were no numerical difficulties experienced with this technique in any calculation, despite the typically rapid readjustment of the location of the boundaries during the early stages of a calculation. To the author's knowledge, this represents the first incorporation of a completely automatic mesh-splitting algorithm with MacCormack's method.

The fourth-order pressure damping term of MacCormack[15] is utilized to prevent numerical instability in the presence of strong shock waves. For the shock-turbulent boundary layer calculation discussed herein, the damping coefficient α was taken to be -0.5, while for the high-speed inlet studies of the subsequent paper[26] a value of -5.0 was used in agreement with previous calculations.[24] In addition, the convective damping technique of MacCormack[14] is incorporated into the $\mathcal{L}_\xi$ operator to prevent occurrence of a nonlinear instability in region of separated flow.

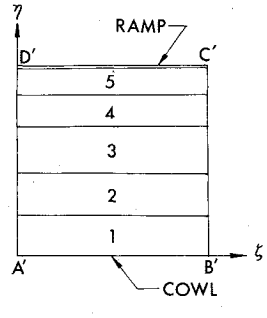

Fig. 3 Subdivision of transformed plane (downstream region shown).

Computational Sublayer

A major factor controlling the efficiency of an explicit finite-difference algorithm such as MacCormack's method is the requirement of resolving all pertinent scales within the ramp and cowl boundary layers. Ordinarily, the exceedingly fine mesh spacing needed to resolve the viscous sublayer portion of the turbulent boundary layers would imply that the allowable time step for integration of Eq. (2) in this region is exceptionally small compared to the allowable time step, for example, in the region outside the boundary layers. This exceptionally large disparity in permissible time steps implies that most of the computer time is spent integrating Eq. (2) over a region comprising a small fraction of the computational domain.

In order to partially alleviate this difficulty, a separate and efficient treatment of the region containing the viscous sublayer and transition portion of the turbulent boundary layer is employed. This region is taken to be $0 \le y' \lesssim 60\nu_w/u_*$, where y' is the distance normal to the wall, $\nu_w = \mu_w/\rho_w$, $u_* = \sqrt{\tau_w/\rho_w}$, with τ_w denoting the wall shear stress and the subscript w implying evaluation at the wall. For lack of better terminology, this region is called the computational sublayer (CSL). Following previous study,[31] the governing equations are taken to be

$$\dot{m}\frac{\partial u'}{\partial y'} = -\frac{\partial p}{\partial x'} + \frac{\partial \tau_{x'y'}}{\partial y'} \tag{10}$$

$$\frac{\partial}{\partial y'}\left[\dot{m}\left(c_pT + \frac{1}{2}u'^2\right) + Q_{y'} - u'\tau_{x'y'}\right] = 0 \tag{11}$$

$$\tau_{x'y'} = (\mu + \epsilon)\frac{\partial u'}{\partial y'} \tag{12}$$

$$Q_{y'} = -c_p\left(\frac{\mu}{Pr} + \frac{\epsilon}{Pr_t}\right)\frac{\partial T}{\partial y'} \tag{13}$$

where x' and y' are local Cartesian coordinates parallel and normal to the surface, respectively; u' is the velocity component parallel to the wall; and $\dot{m}$ is the normal mass flux at the surface (boundary-layer bleed implying negative values of $\dot{m}$). The orientation of the computational sublayer coordinates for the $\eta = 0$ boundary is illustrated in Fig. 4. A similar development is provided for the $\eta = 1$ boundary. These equations are obtained from Eq. (2) under the following assumptions: 1) negligible streamwise variation in the convection of mass, momentum, and total enthalpy within the computational sublayer, i.e.,

$$\frac{\partial \rho u'}{\partial x'} \approx 0, \frac{\partial \rho u'^2}{\partial x'} \approx 0$$

and

$$\frac{\partial}{\partial x'}\left\{\rho u'\left[c_pT + \frac{1}{2}(u'^2 + v'^2)\right]\right\} \approx 0$$

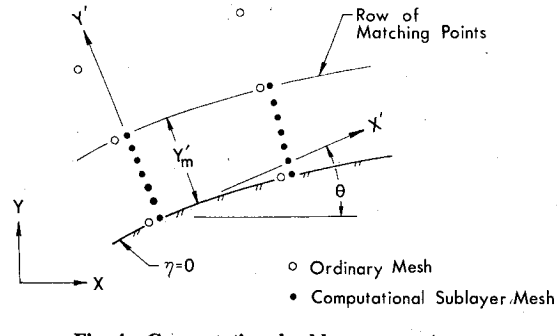

Fig. 4 Computational sublayer geometry.

where v' is the velocity component normal to the wall; 2) boundary-layer approximation; 3) height of CSL small compared to the radius of curvature of the wall; 4) negligible variation in $\partial p/\partial x'$ across the CSL; and 5) $v'^2 \ll 2c^2/(\gamma-1)$, where $c=\sqrt{\gamma RT}$ is the local speed of sound. The validity of these five assumptions has been successfully demonstrated for a flat plate adiabatic turbulent boundary layer and a shock-turbulent boundary layer interaction, with the latter case displaying flow separation. Details are provided in the next section.

The application of the CSL modification is illustrated in Fig. 4 for the $\eta=0$ boundary. Two different sets of mesh points are evident. First, the set of mesh points on which MacCormack's algorithm is applied (denoted as the ordinary mesh) is shown as the open circles. Between the row of ordinary points adjacent to the wall (denoted as the row of matching points) and the wall itself, a second set of mesh points (denoted by the computational sublayer mesh) is indicated as the darkened circles. The height y'_m of the row of matching points above the wall is typically less than $60\,\nu_w/u_*$. Since the quantities ν_w and u_* are not known a priori, an estimate is made for ν_w/u_* at each point along the wall, and the distance y'_m is controlled during the generation of the ordinary mesh. Since Eqs. (10-13) have been found to be valid for $y' \lesssim 60\nu_w/u_*$ (see next section), the precise value obtained for $y'_m u_*/\nu_w$ when the flowfield is converged is unimportant provided it is generally less than 60.

The mesh spacing for the ordinary points provides sufficient resolution of all pertinent flow features, except at the row of matching points. Specifically, in updating the flow variables on the row of matching points near $\eta=0$, among the quantities required are the components of the Cartesian stress tensor $\tau_{xx},\tau_{xy},\tau_{yy}$ and heat flux vector Q_x,Q_y at the wall (in the predictor step of the $\mathcal{L}_\eta$ operator) and at the row of matching points (in the corrector step of the $\mathcal{L}_\eta$ operator and both steps of the $\mathcal{L}_\xi$ operator). In these specific instances, the η derivatives of the velocity and temperature components ordinarily would be approximated using values at $j=1$ (the wall) and $j=2$ (the row of matching points) or $j=1$ and $j=3$ depending on the operator. However, with the computational sublayer technique the mesh spacing y'_m is substantially greater than the viscous sublayer thickness and such an approximation for the derivatives would be highly inaccurate. Instead, the computational sublayer technique is used to provide accurate values for $\tau_{xx},\tau_{xy},\tau_{yy},Q_x$ and Q_y when updating the flowfield at the row of matching points. The components of the Cartesian stress tensor are obtained from the sublayer solution by a simple coordinate transformation, under the reasonable assumption that the normal stresses in the x',y' coordinate system (i.e., $\tau_{x'x'}$ and $\tau_{y'y'}$) are small compared to $\tau_{x'y'}$. Referring to the $\eta=0$ boundary in Fig. 4,

$$\tau_{xx} = -\tau_{yy} = -2\sin\Theta\cos\Theta\ \tau_{x'y'}$$

$$\tau_{xy} = (\cos^2\Theta - \sin^2\Theta)\,\tau_{x'y'} \tag{14}$$

where Θ is the angle of inclination of the boundary relative to the x axis. Similarly, the components of the heat transfer vector are obtained assuming $Q_{y'} \gg Q_{x'}$, and thus

$$Q_x = -\sin\Theta\ Q_{y'}, \quad Q_y = \cos\Theta\ Q_{y'} \tag{15}$$

Expressions can be similarly derived for the computational sublayer on $\eta=1$.

The CSL region is solved during each updating of the adjacent region of the ordinary mesh, with the pressure gradient $\partial p/\partial x'$ in Eq. (10) obtained from the pressure distribution on the row of matching points. The procedure consists of two parts. First, the temperature distribution in the CSL is held fixed at its value from the previous step and Eq. (10) is solved for u' subject to the boundary conditions $u'=0$ at $y'=0$ and $u'=u'_m$ at $y'=y'_m$, where u'_m is the value of u' at $y'=y'_m$ obtained from the velocity on the row of matching points. In the cases discussed herein and in the subsequent paper,[26] the CSL turbulent eddy viscosity was also fixed at its value from the previous step. A closed form expression for the wall shear stress τ_w is obtained by integrating Eq. (10) twice and is evaluated numerically. The first integral of Eq. (10) then provides a first-order differential equation for u' involving τ_w that is solved numerically by the trapezoidal rule. The sublayer eddy viscosity is then updated. Recently, the numerical code was modified to solve Eq. (10) as a nonlinear two-point boundary-value problem[32] using the second-order accurate box scheme[33] (centered Euler scheme) and Newton iteration, holding only the temperature distribution in the CSL fixed at its value from the previous step. Comparison of these two approaches for a typical high-speed inlet calculation showed virtually identical results, with the box scheme approach affording a slight improvement in the rapidity of convergence of the overall flowfield to steady state. In the second part of the procedure, the CSL temperature is obtained from Eq. (11) subject to the boundary conditions $\partial T/\partial y'=0$ at $y'=0$ (adiabatic wall) and $T=T_m$ at $y'=y'_m$, where T_m is the temperature at the row of matching points. Equation (11) may be integrated twice analytically to yield a closed form expression for the wall temperature T_w that is evaluated numerically. The first integral of Eq. (11) then provides a first-order differential equation for T involving T_w, that is solved numerically by the trapezoidal rule. The components of the Cartesian stress tensor and heat flux vector at the wall and the row of matching points are obtained from Eqs. (12-15). A variety of test calculations were performed that indicated the CSL region was updated sufficiently often to insure that the sublayer flow was converged by the time the ordinary flow had achieved a steady state.

The CSL modification is somewhat similar to previous work by Baldwin and MacCormack[34] and Baldwin and Lomax.[35] In the former case, an iterative technique was employed using the full boundary-layer equations to provide values of all variables at the second row of ordinary mesh points from the wall. The method differs from the present technique principally in its inclusion of the streamwise flux terms, e.g., $\partial\rho u'/\partial x'$, which were found in all present calculations to be insignificant (see next section). A similar conclusion was reached by Baldwin and MacCormack. The latter technique of Baldwin and Lomax differs from the present method in its assumption that $\tau_{x'y'}$ is constant throughout the sublayer (taken to be $0<y'_m \lesssim 50\nu_w/u_*$ in Ref. 35) which is invalid in the presence of large streamwise pressure gradients. In addition, the present method has been generalized to include the effects of boundary-layer bleed and curvilinear wall geometry.

Verification of Computational Sublayer Modification

Prior to application of the numerical method to the computation of high-speed inlet flows it was deemed necessary to evaluate two major aspects of the CSL modification, specifically the sensitivity of the computed flow to the height of the sublayer region y'_m and the accuracy of the technique for separated flows. The results are indicated in the following section.

Flat Plate Turbulent Boundary Layer

The sensitivity of the computed flow to the particular value of the nondimensional sublayer height $y'_m u_*/\nu_w$ was considered for the simple configuration of a turbulent boundary layer on an adiabatic flat plate at a freestream Mach number $M_\infty=2.96$, total temperature $T_{t\infty}=243$ K (437°R), and total pressure $p_{t\infty}=377.2$ kPa (54.7 psia). This configuration corresponds to the region upstream of the shock-turbulent boundary-layer interaction discussed later. A total of four cases were considered. The first three cases employed the CSL modification, while in the fourth case the CSL modification

was not employed and the viscous sublayer was resolved using the ordinary mesh in the conventional manner. For the first three cases, the height of the computational sublayer y'_m was varied in order to determine the effect on the computed flowfield. In each case, a constant streamwise mesh spacing $\Delta x = 1.56\,\delta$ was employed, where $\delta = 0.33$ cm (0.13 in.) is the boundary-layer thickness at $x = 13.7$ cm (5.40 in.) which is near the the downstream boundary of the computational domain. Near the wall, the ordinary mesh points were stretched geometrically in y according to

$$\Delta y_j = y_j - y_{j-1} = C\Delta y_{j-1}, \quad j = 3,4,\ldots,JM \tag{16}$$

where y_j is the physical location of the jth point from the wall (with $y_1 = 0$), the $\Delta y_2 = y'_m$ is the CSL height, C is the geometric stretching factor, and JM is the number of points in the geometrically stretched region. Outside this region the mesh spacing in y was uniform. The details of the mesh distribution are given in Table 1.

As indicated in Table 1, for cases 1-3 the nondimensional sublayer height $y'_m u_*/\nu_w = \Delta y_2^+$ was 27.8, 52.1, and 97.3, respectively, with corresponding dimensionless CSL spacing Δy_{SL}^+ of 3.09, 5.79, and 10.8, which is sufficient to resolve the viscous sublayer (the mesh spacing $\Delta y_{SL}^+ = 10.8$ in case 3 is somewhat larger than that normally desired for resolution of the viscous sublayer, which is typically $\Delta y_{SL}^+ \lesssim 5$). In case 4, where the CSL modification was not used, the dimensionless mesh spacing at the wall $\Delta y_2^+ = 3.8$ provided adequate resolution of the viscous sublayer.

The computed skin friction coefficient c_f for the four cases is indicated in Fig. 5. Except in the immediate vicinity of the leading edge, the values for all four cases are in close agreement. For example, at $x = 13.7$ cm (5.4 in.), corresponding to $Re_x = \rho_\infty U_\infty x/\mu_\infty = 5.40 \times 10^6$, the average value of c_f for the four cases is 1.737×10^{-3}, with a maximum deviation of 2%. The results are in close agreement with the values predicted for c_f using the Van Driest II theory together with the Kármán-Schoenherr equation.[36] In particular, the values of c_f for cases 1 and 4, which are essentially identical for $x > 3.1$ cm (1.2 in.) are within 6.9% the Kármán-Schoenherr value at $x = 7.9$ cm (3.1 in.), and within 2.7% of the Kármán-Schoenherr value at $x = 13.7$ cm (5.4 in.); these locations correspond to a momentum thickness Reynolds number of 5900 and 7700, respectively.

The CSL modification substantially improves the efficiency of the numerical code. The computer time required for each of the three cases that used the CSL modification represents a decrease by a factor of between 7.8 and 8.3 compared to the time required for case 4, which did not utilize the CSL modification.

In summary, the numerical algorithm with the CSL technique has been shown to provide accurate flowfield solutions with a substantial improvement in computational efficiency. Based on these calculations, the following somewhat conservative criterion has been adopted for the maximum height of the CSL region:

$$y'_m \lesssim 60\nu_w/u_* \tag{17}$$

Table 1 Mesh distribution for flat plate turbulent boundary layer

Case	Type	IL	JL	JSL	JM	C	Δy_2^+	Δy_{SL}^+
1	CSL	32	32	10	21	1.154	27.8	3.09
2	CSL	32	28	10	19	1.198	52.1	5.79
3	CSL	32	30	10	20	1.145	97.3	10.8
4	No CSL	32	35	—	30	1.200	3.8	—

IL = number of mesh points in x direction. JL = number of ordinary mesh points in y direction. JSL = number of mesh points in CSL. JM = number of mesh points in geometrically stretched region. C = geometric stretching factor. $\Delta y_2^+ = \Delta y_2 u_*/\nu_w$, where Δy_2 is distance above wall of first row of ordinary points; u_* and ν_w are evaluated at $x = 13.7$ cm. $\Delta y_{SL}^+ = \Delta y_{SL} u_*/\nu_w$, where Δy_{SL} is distance above wall of first row of computational sublayer points.

The computed results for a flat plate boundary layer have been shown to be insensitive to the particular value of y'_m employed within the above limit.

Shock/Turbulent Boundary-Layer Interaction

The purpose of this phase of the research is to demonstrate the capability of the numerical algorithm with the CSL modification to accurately compute flows displaying shock/turbulent boundary-layer interaction and flow separation. The configuration chosen is the interaction of an oblique shock wave with a turbulent boundary layer on an adiabatic flat plate. The freestream Mach number M_∞ is 2.96, and the freestream total temperature and total pressure are 243 K (437°R) and 377.2 kPa (54.7 psia), respectively. An oblique shock wave at an angle of 25.84 deg with respect to the horizontal intersects the plate at a distance $x_{SHK} = 30.5$ cm (12 in.) from the leading edge. The Reynolds number based on freestream conditions and the length x_{SHK} is 1.2×10^7. This configuration has been investigated experimentally by Law[37] and computed by Shang, et al.[17] The calculations of Shang employed MacCormack's explicit method, and directly resolved the viscous sublayer without use of the CSL modification.

The calculation was performed in two steps. First, the region upstream of the shock/boundary-layer interaction extending from $x = -1.83$ cm (-0.72 in.) to $x = 30.5$ cm (12 in.) was computed. The profiles at $x = 26.6$ cm (10.5 in.) were then employed as the upstream condition for the calculation of the shock/boundary-layer interaction (SBLI) region extending from $x = 26.6$ to 34.2 cm (10.5 to 13.5 in.). This overlapping procedure is identical to that employed by Shang. The details of the mesh distribution are given in Table 2 where u_* and ν_w are evaluated at $x = 26.5$ cm (10.4 in.) and $\delta = 0.43$ cm (0.17 in.) is the boundary-layer thickness at $x = 26.5$ cm (see Table 1 for definition of terms).

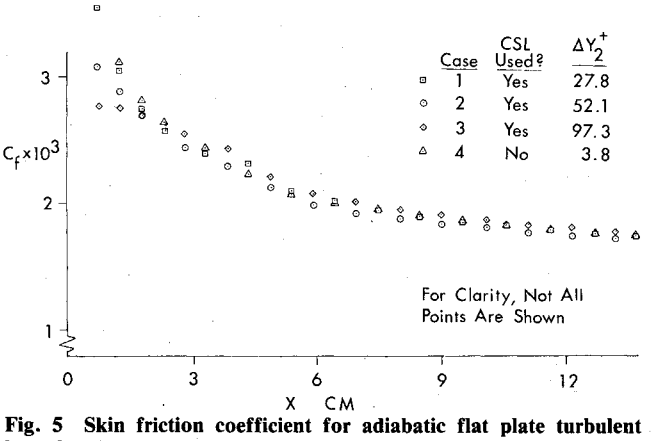

Fig. 5 Skin friction coefficient for adiabatic flat plate turbulent boundary layer.

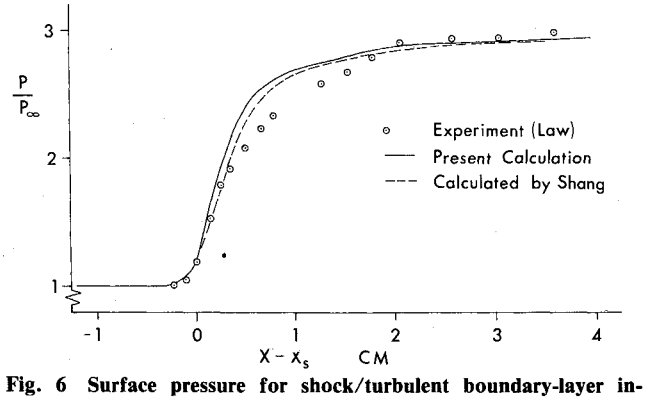

Fig. 6 Surface pressure for shock/turbulent boundary-layer interaction.

Table 2 Mesh distribution for shock/turbulent boundary-layer interaction

Case	Type	*IL*	*JL*	*JSL*	*JM*	*C*	$\Delta x/\delta$	Δy_2^+	Δy_{SL}^+
Upstream of SBLI	CSL	64	30	10	19	1.154	1.20	24.2	2.69
SBLI region	CSL	64	30	10	19	1.154	0.28	24.2	2.69
Shang et al.[17] (SBLI region)	No CSL	64	30	—	18	Variable	0.28	9.6	—

The computed results in the upstream region are in close agreement with the calculations of Shang. In particular, the computed value of c_f at $x=26.6$ cm (10.5 in.) (the restart station) is 1.569×10^{-3}, while the value of Shang at the same location is 1.527×10^{-3}. The computed adiabatic wall temperature at the same location is 226.2 K (407.1°R) which compares favorably with the theoretical value of 227.5 K (409.5°R) obtained from the expression[38]

$$T_w = T_\infty\left(1+\frac{(\gamma-1)}{2}Pr_t M_\infty^2\right) \tag{18}$$

The predicted value of Shang is 209.4 K (376.9°R). The disagreement between this value and the theoretical value from Eq. (18) possibly may be attributed to the fact that the value $\Delta y_2^+=9.6$ in Shang's calculation is approximately 3.6 times the effective finer mesh spacing at the wall employed in the present case (i.e., $\Delta y_{SL}^+=2.69$).

In Fig. 6, the computed surface pressure is compared with the previous calculation of Shang and the experimental data of Law. The abscissa is $x-x_s$, where x is the streamwise distance and x_s is the location of the separation point. The computed separation point, obtained by linear interpolation of c_f, is $x_s=29.96$ cm (11.80 in.) which is in close agreement with the value $x_s=30.02$ cm (11.82 in.) obtained by Shang. The pressure calculations are in close agreement, thereby providing additional confirmation of the accuracy of the CSL modification. There is some disagreement with the experimental results ahead of the peak in the pressure, which may be attributed to the approximate nature of the turbulence model and uncertainty in the experimental measurements.[17]

The computed skin friction coefficient c_f is presented in Fig. 7, together with the previous results of Shang and the experimental separation-to-reattachment length of Law. The results are in close agreement, particularly in the extent of the separation region. The present results, however, indicate a larger peak negative skin friction and slightly greater values downstream of reattachment. These differences may be attributed to the fact that in the present case an effective finer mesh resolution is employed near the wall.[39]

In order to evaluate the effect of the approximations employed in the sublayer model, the full boundary-layer equations may be integrated across the sublayer region $0\le y\le y'_m$ to yield the following general expression for the wall shear stress:

$$\tau_w = T_1 + T_2$$

$$T_1 = \left[u'_m - \frac{\partial p}{\partial x}\int_0^{y'_m}\frac{y\,dy}{(\mu+\epsilon)} - \dot{m}\int_0^{y'_m}\frac{u\,dy}{(\mu+\epsilon)}\right]\Big/ f(y'_m)$$

$$T_2 = -\left\{\int_0^{y'_m}\frac{1}{(\mu+\epsilon)}\left[(\rho v-\dot{m})u+\int_0^y\frac{\partial}{\partial x}(\rho u^2)\,dy\right]dy\right\}\Big/ f(y'_m)$$

$$f(y'_m) = \int_0^{y'_m}\frac{dy}{(\mu+\epsilon)} \tag{19}$$

where u'_m is the velocity at y'_m and $\dot{m}$ is the bleed mass flux, which is zero in this case. The first term is equivalent to the expression employed for τ_w in the sublayer model, and the second term represents the correction to the wall shear stress due to the terms neglected in the sublayer equations. Using the computed solution, this second term was evaluated, and the corrected value of the friction coefficient is displayed in Fig. 7. It is evident that the corrections to the wall shear stress are negligible everywhere, including the region of separated flow. A similar analysis was performed for the wall temperature, and the maximum correction was found to be 0.63%.

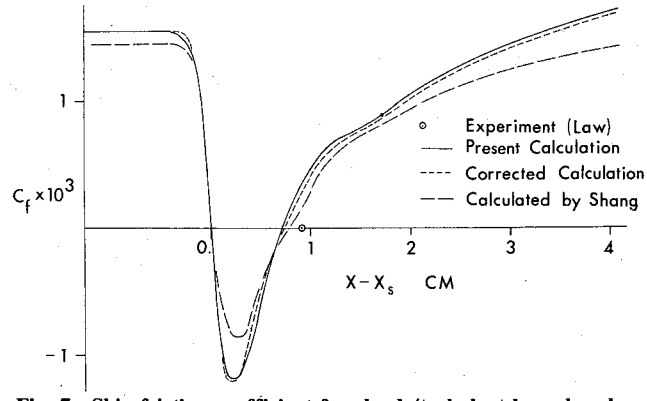

Fig. 7 Skin friction coefficient for shock/turbulent boundary-layer interaction.

In summary, the use of the CSL technique has been shown to provide accurate solutions of flowfields with shock/turbulent boundary-layer interaction, including regions of separated flows. In a subsequent paper,[26] the numerical algorithm is applied to the calculation of three different configurations of a simulated high-speed inlet.

Conclusions

An improved numerical capability has been developed for the computation of two-dimensional high-speed inlets using the Navier-Stokes equations, with turbulence represented by an algebraic turbulent eddy viscosity. A curvilinear body-oriented coordinate system is utilized to facilitate treatment of arbitrary inlet contours. Provision is included for the general specification of boundary-layer bleed on the ramp and cowl surfaces. The numerical algorithm of MacCormack is employed to solve the Navier-Stokes equations. A number of traditional techniques are utilized to improve computational efficiency, including time splitting of the finite-difference operators, splitting of the mesh into several regions in the cross-streamwise direction, and overlapping of successive computational regions. A novel automatic procedure has been developed for optimization of the mesh splitting. A modified treatment of the viscous sublayer and transition portions of the turbulent boundary layer denoted the computational sublayer (CSL) has been introduced.

The accuracy and efficiency of the numerical algorithm with the CSL modification has been investigated for an adiabatic flat plate turbulent boundary layer and a shock/turbulent boundary-layer interaction. In the former case, the results obtained using the numerical algorithm with the CSL modification are in excellent agreement with those obtained by the conventional approach, while achieving an approximate factor of eight reduction in computer time. In the latter case, good agreement was obtained with ex-

perimental data and the previous calculation of Shang. The correction to the wall shear stress and temperature due to the neglected terms in the sublayer model was estimated and found to be negligible.

Acknowledgment

This research was performed through sponsorship of the Air Force Flight Dynamics Laboratory under AF Contract F33615-78-C-3008.

References

[1] Antonatos, P., Surber, L., and Stava, D., "Inlet/Air Plane Interference and Integration," *Airframe/Engine Integration*, AGARD LS-53, May 1972.

[2] Sorensen, V., "Computer Program for Calculating Flow Fields in Supersonic Inlets," NASA TN D-2897, 1965.

[3] Vadyak, J. and Hoffman, J., "Calculation of the Three-Dimensional Flow Field in Supersonic Inlets at Angle of Attack Using a Bicharacteristic Method with Discrete Shock Fitting," AIAA Paper 79-0379, Jan. 1979.

[4] Presley, L., "A Comparison of a Shock-Capturing Technique with Experimental Data for Three-Dimensional Internal Flows," *Aerodynamic Analyses Requiring Advanced Computers,* NASA SP-347, 1975, pp. 623-642.

[5] Sorensen, N., Smeltzer, D., and Latham, E., "Advanced Supersonic Inlet Technology," *Journal of Aircraft*, Vol. 10, May 1973, pp. 278-282.

[6] Reyhner, T. and Hickcox, T., "Combined Viscous-Inviscid Analysis of Supersonic Inlet Flowfields," *Journal of Aircraft*, Vol. 9, Aug. 1972, pp. 589-595.

[7] Sorensen, N. and Smeltzer, D., "Performance Estimates for a Supersonic Axisymmetric Inlet System," *Journal of Aircraft*, Vol. 9, Oct. 1972, pp. 703-706.

[8] Syberg, J. and Koncsek, J., "Experimental Evaluation of an Analytically Derived Bleed System for a Supersonic Inlet," *Journal of Aircraft*, Vol. 13, Oct. 1976, pp. 792-797.

[9] Gros, A., Watson, E., Seebaugh, W., Sanator, R., and DeCarlo, J., "Investigation of Flow Fields within Large-Scale Hypersonic Inlet Models," NASA TN D-7150, 1973.

[10] Surber, L. and Sedlock, D., "Effects of Airframe-Inlet Integration on Half-Axisymmetric and Two-Dimensional Supersonic Inlet Performance," AIAA Paper 78-960, July 1978.

[11] Lubard, S. and Helliwell, W., "Calculation of the Flow on a Cone at High Angle of Attack," *AIAA Journal*, Vol. 12, July 1974, pp. 965-974.

[12] Vigneron, Y., Rakich, J., and Tannehill, J., "Calculation of Supersonic Viscous Flow Over Ogive Cylinders at Angle of Attack," AIAA Paper 79-0131, Jan. 1979.

[13] Buggeln, R., McDonald, H., Kreskovsky, J., and Levy, R., "Computation of Three-Dimensional Viscous Supersonic Flow in Inlets," AIAA Paper 80-0194, Jan. 1980.

[14] MacCormack, R., "Numerical Solution of the Interaction of a Shock Wave with a Laminar Boundary Layer," *Lecture Notes in Physics*, Vol. 8, 1971, pp. 151-163.

[15] MacCormack, R. and Baldwin, B., "A Numerical Method for Solving the Navier-Stokes Equations with Application to Shock-Boundary Layer Interactions," AIAA Paper 75-1, Jan. 1975.

[16] Shang, J. and Hankey, W. L., Jr., "Numerical Solution for Supersonic Turbulent Flow Over a Compression Ramp," *AIAA Journal*, Vol. 13, Oct. 1975, pp. 1368-1374.

[17] Shang, J., Hankey, W. L., Jr., and Law, C., "Numerical Simulation of Shock Wave-Turbulent Boundary Layer Interaction," *AIAA Journal*, Vol. 14, Oct. 1976, pp. 1451-1457.

[18] Hung, C. and MacCormack, R., "Numerical Solution of Three-Dimensional Shock Wave and Turbulent Boundary-Layer Interaction," *AIAA Journal*, Vol. 16, Oct. 1978, pp. 1090-1096.

[19] Shang, J., "Implicit-Explicit Method for Solving the Navier-Stokes Equations," *AIAA Journal*, Vol. 16, May 1978, pp. 496-502.

[20] Beam, R. and Warming, R., "An Implicit Factored Scheme for the Compressible Navier-Stokes Equations," *AIAA Journal*, Vol. 16, April 1978, pp. 393-402.

[21] Steger, J., "Implicit Finite-Difference Simulation of Flow About Arbitrary Two-Dimensional Geometries," *AIAA Journal*, Vol. 16, July 1978, pp. 679-686.

[22] Steger, J. and Bailey, H., "Calculation of Transonic Aileron Buzz," *AIAA Journal*, Vol. 18, March 1980, pp. 249-255.

[23] Knight, D. and Hankey, W. L., Jr., "Numerical Simulation of Nonchemically Reacting Radial Supersonic Diffusion Laser," AIAA Paper 76-60, Jan. 1976.

[24] Knight, D., "Numerical Simulation of Realistic High Speed Inlets Using the Navier-Stokes Equations," *AIAA Journal*, Vol. 15, Nov. 1977, pp. 1583-1589.

[25] Chaussee, D. and Pulliam, T., "A Diagonal Form of an Implicit Approximate-Factorization Algorithm with Application to a Two Dimensional Inlet," AIAA Paper 80-0067, Jan. 1980.

[26] Knight, D., "Improved Calculation of High Speed Inlet Flows: Part II. Results," *AIAA Journal*, to be pubished.

[27] Thompson, J., Thames, F., and Mastin, C., "Automatic Numerical Generation of Body-Fitted Curvilinear Coordinate System for Field Containing Any Number of Arbitrary Two-Dimensional Bodies," *Journal of Computational Physics*, Vol. 15, July 1974, pp. 299-319.

[28] Knight, D., "Improved Numerical Simulation of High Speed Inlets Using the Navier-Stokes Equations," AIAA Paper 80-0383, Jan. 1980.

[29] Rubesin, M. and Rose, W., "The Turbulent Mean-Flow, Reynolds-Stress and Heat-Flux Equations in Mass Averaged Dependent Variables," NASA TMX-62248, March 1973.

[30] Cebeci, T. and Smith, A.M.O., *Analysis of Turbulent Boundary Layers*, Academic Press, New York, 1974.

[31] Cebeci, T., "Calculations of Compressible Turbulent Boundary Layers with Heat and Mass Transfer," *AIAA Journal*, Vol. 9, June 1971, pp. 1091-1097.

[32] Knight, D., "Calculation of High Speed Inlet Flows Using the Navier-Stokes Equations," AIAA Paper 80-1107, June 1980.

[33] Keller, H., "Accurate Difference Methods for Nonlinear Two-Point Boundary Value Problems," *SIAM Journal of Numerical Analysis*, Vol. 11, April 1974, pp. 305-320.

[34] Baldwin, B. and MacCormack, R., "Numerical Solution of the Interaction of a Strong Shock Wave with a Hypersonic Turbulent Boundary Layer," AIAA Paper 74-558, June 1974.

[35] Baldwin, B. and Lomax, H., "Thin Layer Approximation and Algebraic Model for Separated Turbulent Flows," AIAA Paper 78-257, Jan. 1978.

[36] Hopkins, E. and Inouye, M., "An Evaluation of Theories for Predicting Turbulent Skin Friction and Heat Transfer on Flat Plates at Supersonic and Hypersonic Mach Numbers," *AIAA Journal*, Vol. 9, June 1971, pp. 993-1003.

[37] Law, C., "Supersonic Shock Wave-Turbulent Boundary Layer Interactions," *AIAA Journal*, Vol. 14, June 1976, pp. 730-734.

[38] Schlichting, H., *Boundary-Layer Theory*, 6th ed., McGraw Hill, New York, 1968, pp. 667-668.

[39] Shang, J., Air Force Flight Dynamics Lab, private communication, June 1979.